

# Halo Histories vs. Galaxy Properties at $z = 0$

## I: The Quenching of Star Formation

Jeremy L. Tinker<sup>1</sup>, Andrew R. Wetzel<sup>2,3,4</sup>, Charlie Conroy<sup>5</sup>, Yao-Yuan Mao<sup>6</sup>

<sup>1</sup>*Center for Cosmology and Particle Physics, Department of Physics, New York University, New York, NY*

<sup>2</sup>*TAPIR, California Institute of Technology, Pasadena, CA*

<sup>3</sup>*Carnegie Observatories, Pasadena, CA*

<sup>4</sup>*Department of Physics, University of California, Davis, CA*

<sup>5</sup>*Department of Astronomy, Harvard University, Cambridge, MA*

<sup>6</sup>*Department of Physics and Astronomy & Pittsburgh Particle Physics, Astrophysics, and Cosmology Center (PITT PACC), University of Pittsburgh, Pittsburgh, PA 15260, USA*

5 March 2024

### ABSTRACT

We test whether halo age and galaxy age are correlated at fixed halo and galaxy mass. The formation histories, and thus ages, of dark matter halos correlate with their large-scale density  $\rho$ , an effect known as assembly bias. We test whether this correlation extends to galaxies by measuring the dependence of galaxy stellar age on  $\rho$ . To clarify the comparison between theory and observation, and to remove the strong environmental effects on satellites, we use galaxy group catalogs to identify central galaxies and measure their quenched fraction,  $f_Q$ , as a function of large-scale environment. Models that match halo age to central galaxy age predict a strong positive correlation between  $f_Q$  and  $\rho$ . However, we show that the amplitude of this effect depends on the definition of halo age: assembly bias is significantly reduced when removing the effects of splashback halos—those halos that are central but have passed through a larger halo or experienced strong tidal encounters. Defining age using halo mass at its peak value rather than current mass removes these effects. In SDSS data, at  $M_* \gtrsim 10^{10} M_\odot/h^2$ , there is a  $\sim 5\%$  increase in  $f_Q$  from low to high densities, which is in agreement with predictions of dark matter halos using peak halo mass. At lower stellar mass there is little to no correlation of  $f_Q$  with  $\rho$ . For these galaxies, age-matching is inconsistent with the data across the wide range the halo formation metrics that we tested. This implies that halo formation history has a small but statistically significant impact on quenching of star formation at high masses, while the quenching process in low-mass central galaxies is uncorrelated with halo formation history.

**Key words:** cosmology: observations—galaxies:clustering—galaxies: groups: general — galaxies: clusters: general — galaxies: evolution

## 1 INTRODUCTION

The abundance matching model for connecting galaxies to halos has proven to be an exceptional tool for understanding both galaxy bias and galaxy evolution (see, e.g., Kravtsov et al. 2004; Conroy et al. 2006; Conroy & Wechsler 2009; Moster et al. 2010, 2013; Behroozi et al. 2013; Reddick et al. 2013). In its simplest form, abundance matching places galaxies within halos based on their relative ranking: the most massive galaxy goes in the most massive, and on down the rank-ordered lists of galaxies and halos. The success of abundance matching suggests a null hypothesis that galaxy properties only care about the mass of their host halo. However, corre-

lations between galaxy and other halo properties at fixed halo mass could manifest in spatial clustering; this is the well-known assembly bias effect, in which halos of fixed mass cluster differently depending on their formation history and internal structure (Gao et al. 2005; Wechsler et al. 2006; Gao & White 2007; Wetzel et al. 2007; Li et al. 2008; Dalal et al. 2008). This idea has been tested in various contexts but with conflicting results.

Using myriad galaxy clustering statistics, a number of studies found no evidence for correlations of galaxy properties with environment at fixed halo mass (Abbas & Sheth 2006; Skibba et al. 2006; Tinker et al. 2008). In contrast, many results using galaxy group catalogs to identify dark matter halos show that galaxy properties depend on

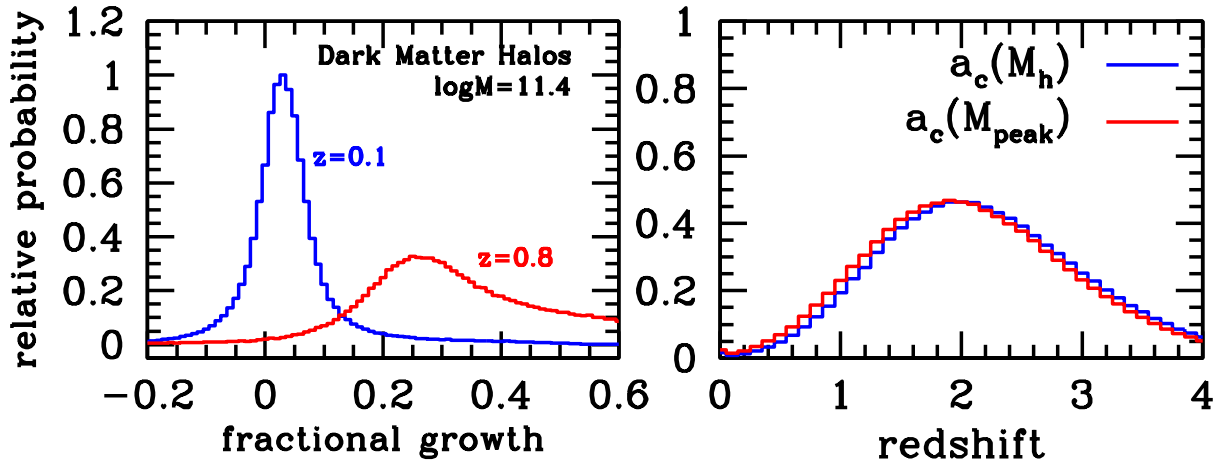


**Figure 1.** *Left Panel:* Fractional growth of halos from  $z = 0.1$  to 0 (blue histogram) and  $z = 0.8$  to 0 (red histogram) for halos of  $\log M_h = 11.4$ . Over the short timeframe of  $z = 0.1 \rightarrow 0$ , a significant fraction of halos exhibit negative growth ( $\sim 20\%$ ). This fraction is negligible for the  $z = 0.8 \rightarrow 0$  timeframe. *Right Panel:* The distribution of halo formation epochs, as defined by the  $a_c$  parameter of Wechsler et al. (2002). The blue histogram shows the standard result when using halo mass as a function of time ( $M_h$ ). The red histogram shows the result when using  $M_{\text{peak}}(z)$  to determine halo growth. See text for details.

halo formation history as well as mass (Yang et al. 2006; Wang et al. 2008, 2013; Lacerna et al. 2014), provided there are no biases in the halo masses induced by the group finding method (Campbell et al. 2015). Kauffmann et al. (2013) find that star formation rates of galaxies in separate halos are correlated, an effect known as ‘galactic conformity’. To model the conformity results, Hearin & Watson (2013) presented the ‘age-matching’ model, in which halos at fixed mass are rank-ordered by their formation time and then abundance matched to color for the galaxies that occupy those halos. Thus the oldest halos contain the reddest galaxies, while to the youngest halos contain the bluest galaxies. A complication of interpreting the age-matching model in the context of galaxy formation is that ‘age’ is quantity difficult to define objectively (Li et al. 2008), and the redshifts at which halos accrue most of their mass may not correlate (or may anticorrelate) with the redshifts at which galaxies form or accrete most of their stars. Additionally, Geha et al. (2012) find a limiting stellar mass of  $10^9 M_\odot/h^2$  for field galaxies, below which no galaxies are quenched. This represents a threshold below which halo formation history can, by definition, play no role in whether a galaxy is quenched because there are none, even though the amplitude of the assembly bias effect only gets stronger as halo mass gets smaller.

In this series of papers, we test the assumption that halo growth and galaxy growth are correlated. We construct this test in several distinct regimes. In this paper, we focus on whether halo growth rate correlates with whether a galaxy is quenched of its star formation and resides on the red sequence. We use the spectral diagnostic  $D_n4000$  to separate galaxies into star-forming and quiescent samples. In a companion paper, we test whether halo growth rate—as well as other galaxy properties—correlates with galaxy star formation rate *within* the star-forming main sequence. Finally, this series will also present new measurements of galactic

conformity in the local universe. To perform these tests, we use group catalogs created from the NYU Value-Added Galaxy Catalog (Blanton et al. 2005), which in turn were created from data from Data Release 7 of the Sloan Digital Sky Survey (York et al. 2000; Abazajian et al. 2009). Results from the group catalogs are compared to models created with high-resolution cosmological N-body simulations. We will focus exclusively on ‘central’ galaxies—galaxies that reside at the center of distinct halos, not orbiting within the virial radius of a larger halo. The latter we classify as satellite galaxies. The formation histories of central and satellite galaxies are quite different and are acted upon by different physical mechanisms (see, e.g., Wetzel et al. 2013 and citations within). To isolate the effect of halo assembly bias on the galaxy population, focusing on central galaxies makes this comparison clearer.

Throughout, we define a galaxy group as any set of galaxies that occupy a common dark matter halo, and we define a halo as having a mean interior density 200 times the background matter density. A *host halo* is a halo that is distinct: its center does not reside within the radius of a larger halo. We will use the terms *halo* and *host halo* interchangeably in this work. A *subhalo* is one whose center is located within the radius of a larger halo. For all distance calculations and group catalogs we assume a flat,  $\Lambda$ CDM cosmology of  $(\Omega_m, \sigma_8, \Omega_b, n_s, h_0) = (0.27, 0.82, 0.045, 0.95, 0.7)$ . Stellar masses are in units of  $M_\odot/h^2$ . We will sometimes refer to galaxies as ‘blue’ and ‘red’ to refer to their intrinsic star formation; ‘red’ means red-and-dead rather than red by dust contamination.

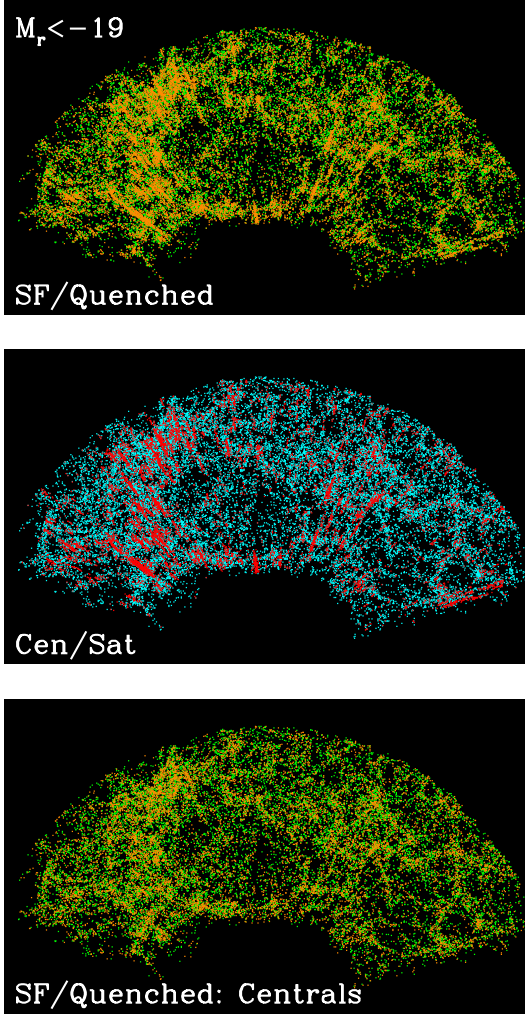


**Figure 2.** *Upper Panel:* A slice through a volume-limited sample of galaxies with  $M_r < -19$ . This sample extends to  $z = 0.064$ . The color types of the points correspond to their star formation activity: the green points are on the star-forming main sequence while the orange points are quiescent galaxies on the red sequence. *Middle Panel:* The same set of galaxies, now categorized as central galaxies and satellite galaxies by the group finder. The group finder clearly identifies the fingers-of-god as redshifted galaxy groups, but some satellites exist in lower density environments. *Lower Panel:* The same as the upper panel, but now only central galaxies are being plotted. With the satellites removed, the finger-of-god effect is ameliorated, but there is a substantial fraction of quiescent galaxies, many of which reside in underdensities and voids.

## 2 DATA, MEASUREMENTS, AND METHODS

### 2.1 NYU Value-Added Galaxy Catalog

To construct our galaxy samples, we use the NYU Value-Added Galaxy Catalog (VAGC; Blanton et al. 2005) based on the spectroscopic sample in Data Release 7 (DR7) of the Sloan Digital Sky Survey (SDSS; Abazajian et al. 2009). We construct four volume-limited samples that contain all galaxies brighter than  $M_r - 5 \log h = -18, -18.5, -19$  and

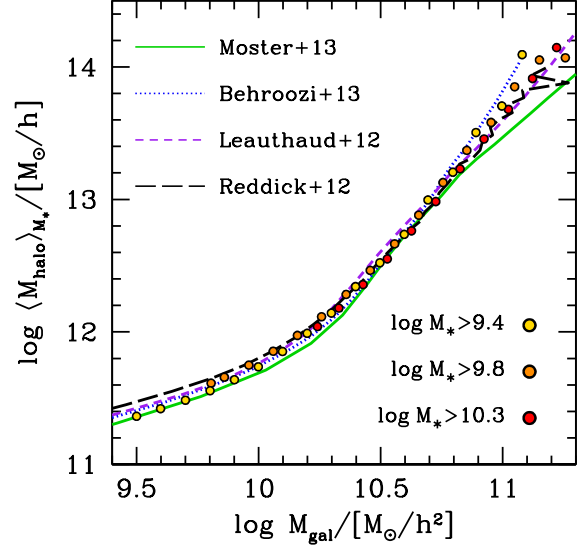


**Figure 3.** Average halo mass in bins of  $\log M_*$  for central galaxies from the three volume-limited group catalogs. The four curves represent a sample of stellar to halo mass relation from abundance matching (Behroozi et al. 2013; Moster et al. 2013) and studies that combine abundance and clustering (Reddick et al. 2013).

$-20$ , respectively. Within each volume-limited sample, we determine the stellar mass at which the sample is complete. The stellar masses are also taken from the VAGC and are derived from the `kcorrect` code of Blanton & Roweis (2007), which assumes a Chabrier (2003) initial mass function. In order of increasing luminosity, the stellar mass samples are complete at  $\log M_* = 9.4, 9.6, 9.8$ , and  $10.3$ , where stellar mass are once again in units of  $M_\odot/h^2$  (see Figure 2 in Tinker et al. 2011).

For galaxy pairs that are too close to obtain spectra because of the 55 arcsecond width of SDSS fibers (‘fiber collisions’), we use the internal correction to the fiber corrections within the VAGC, namely that the collided object is given the redshift of the nearest galaxy in terms of angular separation, provided that this redshift is in agreement with the photometric redshift obtained by with the SDSS photometry (Blanton et al. 2005).

Using galaxy color as a proxy for star formation activity can be problematic, as dust reddening can cause a gas-rich disk galaxy to be classified as a red sequence object (Maller et al. 2009; Masters et al. 2010). To avoid this problem, we use both  $D_n4000$ , which is a diagnostic of the light-weighted age of the stellar population and thus is sensitive to the integrated star formation history of the galaxy. We obtain these quantities from the JHU-MPA spectral reductions<sup>1</sup> (Brinchmann et al. 2004).

### 2.2 Measuring Large-scale Environment

For each galaxy, we estimate the large-scale environment by counting the number of neighboring galaxies within a sphere

<sup>1</sup> <http://www.mpa-garching.mpg.de/SDSS/DR7/>

of radius  $10 h^{-1}$  Mpc centered on each galaxy. This quantity is a biased indicator of the dark matter density field, but at  $10 h^{-1}$  Mpc this bias is a simple linear factor and any stochasticity is minimal. We count the number of galaxies above the corresponding magnitude threshold for the each sample, and so the tracer of the density field has a different bias for each sample. We do not correct for this between the samples, but note that the relative bias between the different samples is at the  $\sim 5\%$  level (Swanson et al. 2008). This galaxy density measurement is affected by galaxy peculiar velocities, but this effect is minimal at  $10 h^{-1}$  Mpc, as we demonstrate in Appendix A in Tinker et al. (2011). We also choose  $10 h^{-1}$  Mpc because represents a clear distinction from a galaxy’s small-scale environment as encapsulated by its host halo. In tests we find that our results show little dependence on the exact smoothing scale chosen. The mean number of galaxies per  $10 h^{-1}$  Mpc sphere is 103, 72, 51, and 21 galaxies for our volume-limited samples, going from faint to bright.

To correct for survey geometry and incompleteness, we use random catalogs. For each volume-limited sample, we produce a catalog of  $10^7$  random points distributed with the angular selection function of SDSS DR7 using the angular mask provided with the VAGC in combination with the software package *mangle* (Swanson et al. 2008). Each random point is also assigned a random redshift such that the comoving space density of randoms is constant with redshift. For each galaxy, we correct for incompleteness by multiplying the observed number of galaxies by the ratio of the number of random points divided by the expected number of randoms if the completeness were unity. The large number of random points ensures that shot noise within each  $10 h^{-1}$  Mpc sphere is at the sub-percent level.

### 2.3 Group Finding Algorithm

We use the halo-based group-finding algorithm presented in Tinker et al. (2011), which is, in turn, based on the algorithm of Yang et al. (2005). In brief, the group finder uses the abundance matching ansatz to assign halo masses to groups, iterated until convergence. The resulting group catalog is a robust decomposition of the entire galaxy population into central galaxies and satellite galaxies. This group finder has been thoroughly vetted in Tinker et al. (2011) as well as Campbell et al. (2015), which specifically investigated color-dependent statistics derived from the group finders. Campbell et al. (2015) concluded that our group finder can robustly identify red and blue centrals and satellites as a function of their stellar mass, but the assignment of halo masses is highly problematic. Thus when using the group catalog, we will only divide the results based on  $M_*$  and not  $M_h$ .

### 2.4 Numerical Simulations and Defining Halo Growth

We compare the results from the group catalog to expectations from dark matter halos. We use the ‘Chinchilla’ simulation (Becker et. al. in prep.), run using a variant of the Gadget-2 cosmological N-body code (Springel 2005) known as L-Gadget2. The box size is  $400 h^{-1}$  Mpc per side, evolving

a density field resolved with  $2048^3$  particles, yielding a mass resolution of  $5.91 \times 10^8 h^{-1} M_\odot$ . The cosmology of the simulation is flat  $\Lambda$ CDM consistent with recent CMB results, with  $\Omega_m = 0.286$ ,  $\sigma_8 = 0.82$ ,  $h = 0.7$ , and  $n_s = 0.96$ . This is slightly higher matter density than assumed for the group catalogs, but the change makes negligible difference in any comparison.

Halos are found in the simulation using the Rockstar code of Behroozi et al. (2013). Halos masses are defined as spherical overdensity masses according to their virial overdensity. We use Consistent Trees (Behroozi et al. 2013) to track the merger and growth history of each halo in the simulation, and we use these histories to determine the growth rate of each halo.

Figure 1 shows the fractional growth of dark matter halos at low mass over different redshift baselines. Halos of this mass are likely to contain galaxies of  $\log M_* = 9.4$ . Detecting assembly bias in survey data has a particular challenge: assembly bias usually increases with decreasing halo mass, but smaller mass halos contain dimmer galaxies are can only be seen in small volumes. The choice of  $\log M_h = 11.4$  represents a compromise between these two effects: halo assembly bias seen in simulations is significant, but SDSS still probes these galaxies at cosmological volumes.

Over the redshift baseline  $z = 0.8 \rightarrow 0$ , halos of this mass scale grow on average  $\sim 30\%$ , but with a wide distribution. Notably, the fraction of halos with negative growth over this timeframe is negligibly small. Over the timeframe of  $z = 0.1 \rightarrow 0$ , the variance in halo growth rates is much smaller, but roughly a quarter of halos lose some mass. Some of this is noise<sup>2</sup>, but these halos exhibit the strong clustering indicative of assembly bias (as we will see in §3), indicating that noise is a minority contributor. Hereafter, we will refer to these redshift baselines as ‘ $\Delta z$ ’. For  $\Delta z = 0.8$ , this definition is over an intermediate timespan ( $\sim 7$  Gyr) over which most of these central galaxies arrive on the red sequence (Tinker et al. 2013). For  $\Delta z = 0.1$ , this definition is sensitive to short-term growth of the dark matter halos. To implement the age-matching model using these definitions, halos are rank ordered from lowest to highest fractional growth. The lowest are considered the oldest, while the halos that have grown the most over that timespan are considered the youngest.

In the right-hand panel, we show the ‘age’ of the same halos as defined by the  $a_c$  parameter from Wechsler et al. (2002), which identifies the epoch where halo growth changes from rapid accretion to slower growth. This is qualitatively similar to using half-mass epoch, although the median of  $z(M_{1/2})$  is lower than that of the median redshift of  $a_c$ . When we quantify assembly bias of halos, we find little difference between using  $z(M_{1/2})$  and  $a_c$ , thus we will focus of

<sup>2</sup> We estimate the noise in assigning halo masses in the Rockstar code by calculating the snapshot-to-snapshot variance around the mean trend in halo growth for each halo for the five snapshots that cover the redshift range  $z = 0.1 \rightarrow 0$ . The variance depends on the order of the polynomial used to fit for the mean trend in  $M_h(z)$ , but for a second-order polynomial the variance is 1.3%. We conclude that this is an upper limit on the noise in estimating halo mass. The variance in the fractional growth is 4%. Assuming Gaussian statistics, removing the contribution from noise would reduce this only to 3.6%.



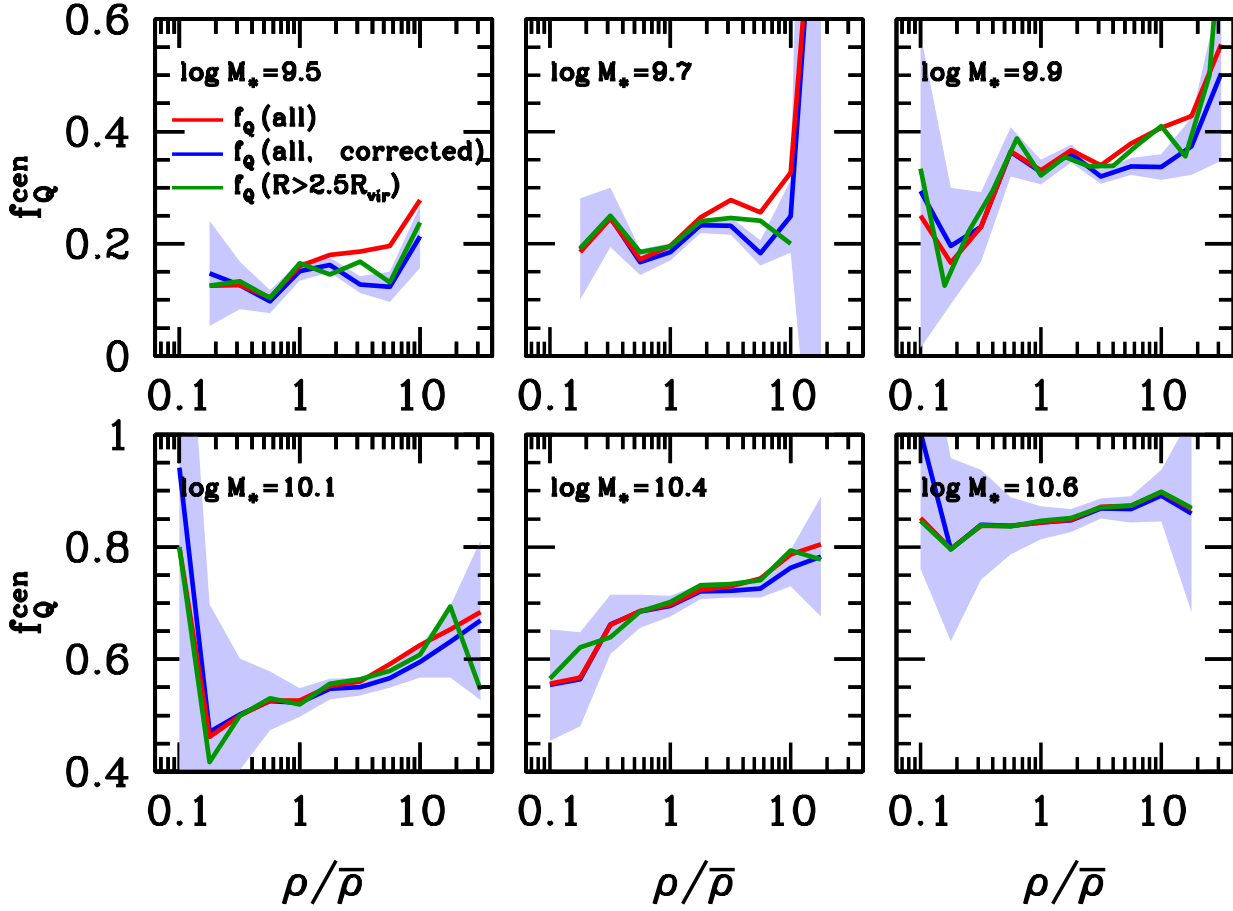


**Figure 4.** Measurements of the quenched fraction of central galaxies,  $f_Q^{\text{cen}}$ , as a function of large-scale density. Each panel shows three methods for measuring  $f_Q^{\text{cen}}$ : (1) The raw measurement that uses all centrals in the group catalog, (2) the measurement using all centrals in the group catalog, but statistically corrected for misidentification of centrals and satellites in the group-finding process, and (3) raw measurement that excludes centrals that are within  $2.5R_{\text{vir}}$  of a larger group. The shaded region around the corrected measurement is the error in the mean, and is representative of the error on the other two measurements. At  $\rho \lesssim 1$ , where the abundance of massive groups is low, all three measurements are essentially the same. At high densities and low stellar masses, the measurements separate at high densities. For high stellar mass bins, the frequency of groups more massive than the host halos being probes is small, and all three measurements are consistent at all  $\rho$ .

$a_c$ . The two histograms in this panel show  $a_c$  for two different definitions of halo mass: (1) the current halo mass at any time,  $M_h(z)$ , and (2) the peak halo mass up to that time  $M_{\text{peak}}(z)$ . As shown in the left-hand panel, over short time intervals there can be significant dark matter mass loss. In fact, small halos can be accreted onto a larger halo but have too much kinetic energy to remain within the larger halo, eventually exiting the larger halo after one pericentric passage. These are called ‘splashback’ halos, and this process can lead to significant stripping of the dark matter halo.  $M_{\text{peak}}(z)$  is a monotonically increasing function, thus for halos that experience tidal stripping,  $M_h(z)$  will be smaller than  $M_{\text{peak}}(z)$ . This has a small but visible impact on the distribution of formation epochs, pushing them to slightly smaller redshift. When rank-ordering halos by their age (or fractional growth), halos that have encountered significant tidal encounters get pushed to the top of the list. Thus, in the standard age-matching model, these halos house the

oldest galaxies. Using  $M_{\text{peak}}$  effectively removes the impact tidal events or splashback galaxies on the ordering of the list. The overall effect on the distribution of halo ages is small, but as we will see in the following section, this choice has a major impact on the predicted assembly bias.

To compare simulation results to galaxy results binned as a function of environment, we measure the density around each halo in the simulation in the same manner as for the galaxies. Using the halo occupation distribution (HOD) fitting results of Zehavi et al. (2011) from the SDSS Main galaxy sample, we populate the simulation with galaxies that match the density and clustering of each of our volume-limited samples. Using the distant-observer approximation and the  $z$ -axis of the box as the line-of-sight, the top-hat redshift-space galaxy densities are measured around each halo.

In an appendix we show the results of two additional proxies for halo age: the redshift at which a halo reaches

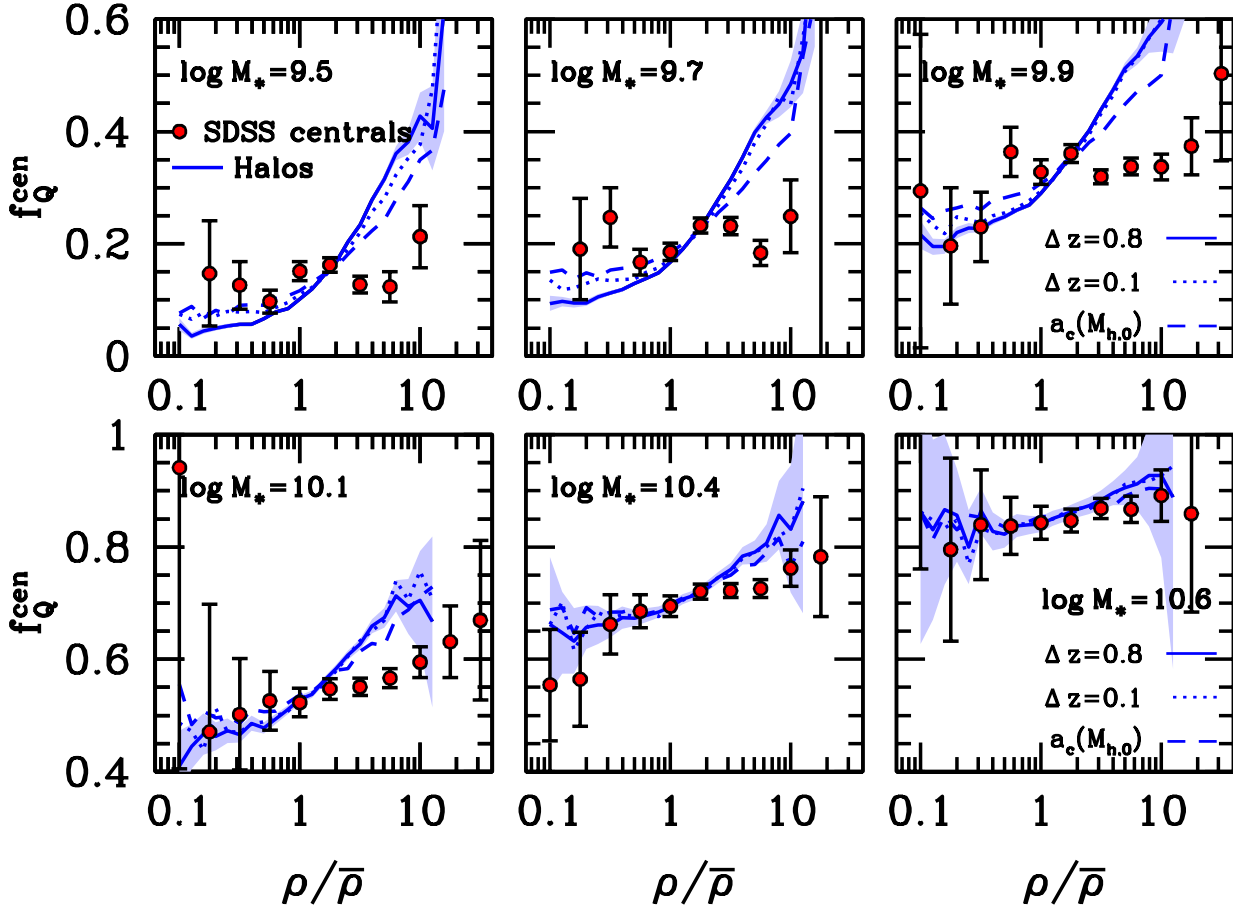


**Figure 5.** The quenched fraction of central galaxies,  $f_Q^{\text{cen}}$ , as a function of large-scale galaxy density, for six bins in  $M_*$ . Galaxy density measurements are described in §2.2. Error bars are the error in the mean in each  $\rho$  bin. In each panel, we compare these measurements to expectations from the age-matching model, which stipulates that redder galaxies (or, in these data, galaxies with the largest values of  $D_n4000$ , which implies that they have the oldest stellar populations) live in older halos. We use the group catalog to estimate the halo masses for each bin in stellar mass. In each bin in halo mass, the halos are rank-ordered by three different definitions of age: (1) their fractional growth since  $z = 0.8$ , (2) their fractional growth since  $z = 0.1$ , and (3) their formation epoch as defined by  $a_c(M_h)$ . We set the break point between ‘old’ and ‘young’ halos to match the value of  $f_Q^{\text{cen}}$  in each bin. As expected from halo assembly bias, the old fraction of halos depends strongly on large-scale environment. The assembly bias gets less strong monotonically with increasing  $M_*$ . The data, in contrast, show the opposite trend. At low stellar masses, there is little to no dependence of  $f_Q$  on environment. As  $M_*$  increases,  $f_Q$  shows a positive trend with  $\rho$ . This figure is an updated version of one presented in Tinker et al. 2011, with new simulation predictions and correcting for an error in the density calculations around the galaxies.

half its present-day mass,  $z_{1/2}$ , and halo concentration,  $c_{\text{vir}}$ , which has been shown to correlate tightly with formation history (Wechsler et al. 2002) and is one of the primary quantities through which halo assembly bias manifests. We do not include these in the main text as they are quantitatively similar to the definitions already in hand. In this appendix, we also show the ‘break points’ delineating old and young halos.

### 3 RESULTS

#### 3.1 Central-satellite decomposition of the SDSS

Figure 2 shows an example of the group finder applied to one of our volume-limited samples. The top panel shows

galaxies in the NGC footprint (only plotting galaxies with  $\delta < 22^\circ$  to avoid crowding), where the color of the point indicates whether the galaxy is star-forming or quiescent. The middle panel shows the same galaxies, but now color indicates whether the galaxy is a central or a satellite. The group catalog clearly identifies the ‘fingers-of-god’ created by the large virial motions of satellite galaxies. Satellites are mostly found in high-density regions along filaments in the cosmic web, although some satellites are still found occasionally out in the field. The bottom panel shows the star-forming and quiescent breakdown of the sample, but now for central galaxies only. Although satellites are more likely to be on the red sequence than central galaxies, this panel elucidates two aspects of central galaxies: (1) the overall fraction of central galaxies on the red sequence is significant at these

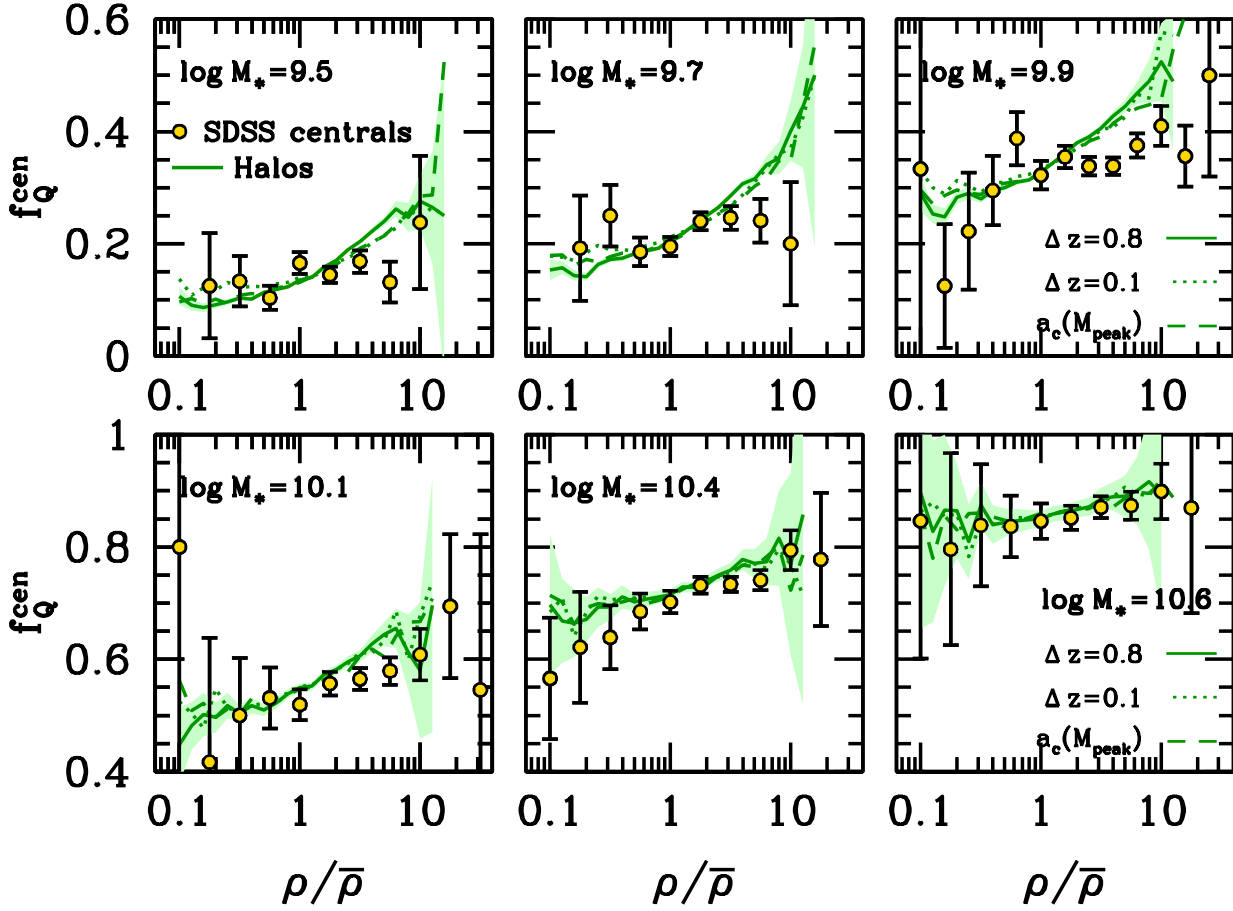


**Figure 6.** Analogous to Figure 5, but removing galaxies that are near larger halos to eliminate the possible effects of splashback encounters. For the data, we remove from the sample any central galaxy that is within  $2.5R_{\text{vir}}$  of a larger halo. The data look nearly the same as in Figure 5, but recall that those data have been statistically corrected for bias in  $f_Q$ , while these data have not been corrected in any way. The three curves show the predictions of the old fraction of dark matter halos. We use the same three definitions of halo age as before. However, for  $\Delta z = 0.8$  and  $\Delta z = 0.1$ , we remove all halos that are within  $2.5R_{\text{vir}}$  of a larger halo, just as with the data. For formation epoch,  $a_c$ , we use  $M_{\text{peak}}$  rather than  $M_h$ , but use all halos in the sample. This removes the impact of tidal events and splashbacks without removing any halos.

masses, and (2) that quenched central galaxies exist at all densities, even the deepest void in the galaxy distribution.

Figure 3 shows the relationship between  $M_h$  and  $M_*$  for central galaxies for three volume-limited group catalogs. The results between the catalogs are in excellent agreement with one another, as well as with results from the literature constraining this relationship from different methods. We use this relationship to make subsequent comparisons between our halo catalogs and the SDSS measurements. Although the mean  $M_h$  in bins of  $M_*$  is not equivalent to the inverse relationship, the differences between Figure 3 and its inverse only appear at  $M_* \gtrsim 10^{10.6}$ , above the limit for our comparisons.

### 3.2 Quenched fraction of central galaxies and large-scale density

The correlation between density and galaxy properties is well-known (see Blanton & Moustakas 2009 and for a thor-

ough review). Progressing from low to high densities, the fraction of galaxies that are red-and-dead,  $f_Q$ , monotonically grows (see, e.g., Oemler 1974; Davis & Geller 1976; Dressler 1980 for canonical works and Hogg et al. 2004; Kauffmann et al. 2004; Blanton et al. 2005; Baldry et al. 2006; Park et al. 2007; Bamford et al. 2009 for more recent measurements). However, this observation combines central galaxies that live in low-mass dark matter halos with satellite galaxies that orbit within high-mass dark matter halos. The observed trend is driven by the density dependence of the halo mass function: more massive halos live in more dense environments, and in turn have a higher fraction of quenched galaxies. The question we pose here is, when restricting the sample to central galaxies of fixed stellar mass, which is a reasonable proxy for fixed halo mass, what is the correlation between  $f_Q$  and environment?

We define red-and-dead galaxies as those with  $D_n4000 > 1.6$ . We find that this value of 1.6 faithfully follows the minimum of the distribution of  $D_n4000$  values be-

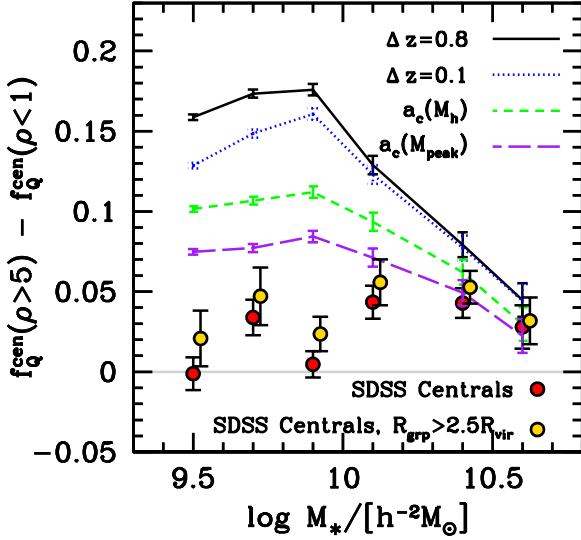


**Figure 7.** Assembly bias in SDSS central galaxies and in dark matter halos. The  $y$ -axis is the difference between the quenched fraction of central galaxies at high densities ( $\rho > 5$ ) and low densities ( $\rho < 1$ ). The red and yellow circles represent SDSS centrals for the full sample (red) and when galaxies near larger groups have been removed (yellow). Recall that the red points have been corrected for biases in the group catalog. Error bars are error in the mean. Curves show predictions from dark matter halos for four different definitions of halo age. We do not show any predictions from age-matching models where halos near groups are removed because they are consistent with the results from the  $a_c(M_{\text{peak}})$  model.

tween the SFMS and the red sequence, irrespective of galaxy stellar mass. We also note that the results are nearly indistinguishable when using sSFR as our indicator of quiescence. Figure 4 shows the quenched fraction of central galaxies,  $f_Q^{\text{cen}}$ , as a function of large-scale galaxy density, measured in three different ways:

- (1) We present the raw measurements of  $f_Q^{\text{cen}}(\rho)$  in which all central galaxies in the group catalog are used.
- (2) We apply a statistical correction to  $f_Q^{\text{cen}}(\rho)$  to remove biases imparted by the group-finding process.
- (3) We measure  $f_Q^{\text{cen}}(\rho)$  after removing all central galaxies that are within  $2.5R_{\text{vir}}$  of a larger group.

For (2),  $f_Q^{\text{cen}}$  is corrected for impurities in the group catalog as in Appendix C in Tinker et al. (2011). In the group-finding process, centrals and satellites are sometimes misclassified, leading to  $\sim 10\%$  of central galaxies in the catalog being true satellites. This effect increases  $f_Q^{\text{cen}}$  because satellite galaxies always have higher quenched fractions at fixed  $M_*$ , and the misclassification occurs more frequently in higher density regions that contain more satellites. The statistical correction described in Tinker et al. (2011) is applied directly to measurements of  $f_Q$ , and robustly accounts for biases in the group-finding process. For  $M_* < 10^{10} M_\odot/h^2$ , the corrected and uncorrected measurements of  $f_Q^{\text{cen}}$  at low densities are the same. This is expected because the abun-

dance of satellite galaxies is negligible at  $\rho < 1$ . At higher  $\rho$ , the correction factor lowers  $f_Q$  by roughly 0.05 to 0.10, also expected from the amount of misclassification in the group catalog (Appendix C in Tinker et al. 2011). At higher stellar masses, the corrected and uncorrected results are consistent at all  $\rho$  due to the fact that there is a smaller difference in the quenched fractions of central and satellite galaxies than for lower  $M_*$ .

For (3), as discussed in §2.4, halo growth can be negative. How this impacts the growth of galaxies is not fully understood, but splashback galaxies are subject to environmental processes, such as ram pressure and strong tidal stripping, that more isolated galaxies are not subjected to. Thus they are not clean tests of the correlation of halo growth history to galaxy formation, and it makes sense to treat them as a separate class of galaxies. Wetzel et al. (2014) showed that splashback galaxies essentially behave the same as satellite galaxies, meaning that after the initial accretion event their evolution is unchanged for a long delay time, and then they rapidly quench their star formation. The key quantity is the time of the initial accretion event, regardless of the previous evolutionary history of the halo; i.e., regardless of whether it was an early-forming halo or late-forming halo before the accretion event. This then begs the question: If splashback galaxies and halos are removed from consideration, what are the observations and theoretical predictions?

To implement (3), we remove all central galaxies with projected separation  $R < 2.5R_{\text{vir}}$  of a larger group and  $\Delta v < 1000$  km/s with respect to the central galaxy of the larger group. These choices are motivated by the results of Wetzel et al. (2014) and references therein. The measurements of  $f_Q^{\text{cen}}$  after this process split the difference between the raw measurements and the corrected measurements. The statistical correction is not applied here because it is only applicable on the full sample of galaxies. But in comparison to the raw data using all centrals, removing galaxies near groups lowers  $f_Q$  in high densities and low stellar masses. For  $M_* \gtrsim 10^{9.8}$  there is little difference between the raw measurements and those with no galaxies near groups.

Regardless of how  $f_Q^{\text{cen}}$  is measured, the results indicate that, at  $M_* < 10^{10} M_\odot/h^2$ , there is little correlation between quenched fraction and large-scale environment. At  $M_* > 10^{10} M_\odot/h^2$ , there is a shallow but significant positive slope of  $f_Q^{\text{cen}}$ . We will compare these results to predictions of the age-matching model in the following sections.

### 3.3 Does halo growth correlate with a galaxy being on the red sequence?

Figure 5 shows the measurements of  $f_Q^{\text{cen}}$ , using all central galaxies and corrected for group-finding biases. The curves show the prediction of the age-matching model, which puts the oldest galaxies into the oldest halos (once fixing halo mass). We choose  $M_h$  by the halo mass assigned to galaxies in each bin, but we note that the halo predictions vary weakly with halo mass (as can be seen in the figure). Thus, minor biases in  $M_h$  and scatter between halo mass and stellar mass are not likely to change the predictions. Halos are rank-ordered by three of the metrics for halo age presented in §2.4: halo growth over the redshift ranges  $\Delta z = 0.8$  and  $\Delta z = 0.1$ , and the formation epoch  $a_c(M_h)$ . We set the



break point between ‘old’ and ‘young’ halos such that the old fraction of halos matches the observed  $f_Q^{\text{cen}}$  in the data.

The age-matching curves in Figure 5 indicate how the fraction of old halos depends on  $\rho$ . Under the age-matching hypothesis—regardless of age definition—the old fraction has a strong dependence on  $\rho$ , with the majority of old halos living in dense environments. This result is consistent with previous results of halo assembly bias, but at odds with the observations at most stellar mass bins, most notably at lower stellar masses. Even at  $M_* > 10^{10} M_\odot/h^2$ , where there is a measurable trend of  $f_Q^{\text{cen}}$  with  $\rho$ , the standard age-matching model predicts a correlation stronger than that seen in the data. At lower masses, the data and theory are at loggerheads: the strength of the assembly bias is at its largest, but the data show the weakest correlation between  $f_Q^{\text{cen}}$  and  $\rho$ , if at all.

### 3.4 Removing the impact of splashback halos and galaxies

Figure 6 shows analogous measurements and models as Figure 5, only here, splashback effects have been removed. For the SDSS central galaxies, any galaxy that is within a projected separation of  $2.5R_{\text{vir}}$  of a larger halo, along with  $\Delta v < 1000$  km/s, is removed from the sample. From Wetzel et al. (2014), this will remove most all splashback galaxies.

The curves in each panel represent the predictions of the age-matching model using the same three definitions of halo age as before. For  $\Delta z = 0.8$  and  $\Delta z = 0.1$ , the halo samples have been altered in the same fashion as the data: all halos within  $2.5R_{\text{vir}}$  of a larger halo have been removed from the sample. In comparison to the age-matching predictions of Figure 5, the assembly bias signal is substantially reduced: there is a definite trend of higher old fraction in higher densities, but not nearly as steep as the trend for all halos. The final age-matching prediction, using  $a_c$ , but now  $a_c$  is defined using  $M_{\text{peak}}$  rather than  $M_h$ . For this model, *no halos are removed* from the catalog. We include this model here, rather than Figure 5, to show that the  $a_c(M_{\text{peak}})$  model induces the same level of assembly bias as models that remove all potential splashback effects.

At lower masses, the age-matching model predicts a correlation of  $f_Q^{\text{cen}}$  with  $\rho$  not seen in the data, although the differences between theory and data are smaller than that seen with the standard age-matching implementation. At higher masses,  $M_* > 10^{10} M_\odot/h^2$ , there is reasonable agreement between the age-matching models and the positive trend of increasing  $f_Q^{\text{cen}}$  with  $\rho$ .

### 3.5 Assembly Bias in Halos and Galaxies

Figure 7 summarizes our results on assembly bias in galaxies and halos. The  $y$ -axis shows the difference between the quenched fractions at high and low densities,  $f_Q^{\text{cen}}(\rho > 5) - f_Q^{\text{cen}}(\rho < 1)$ , as a function of stellar mass. At low masses, the results are generally consistent with little to no assembly bias. At high masses, there is a statistically robust assembly bias signal, with red fractions being around 0.05 higher at high densities. The overall quenched fraction at these masses approaches unity, thus another way to phrase the result is

that the *blue fraction* of central galaxies in high densities is 10-20% lower than in lower densities.

The curves show the predictions of the age-matching models for four different age definitions. The first three show the models from Figure 5, in which all halos are used at each mass bin. The fourth model uses  $a_c(M_{\text{peak}})$  as the halo age definition, although we note that all the theoretical models from Figure 6 are consistent with one another. At low stellar mass, Figure 7 conveys two important points: 1) that the amplitude of the assembly bias signal depends strongly on how one defines halo age, and 2) that none of these models are in particularly good agreement with the data. At high stellar masses, the comparison of halos and galaxies is quite different. There is still a dependence of the assembly bias signal on age definition, but the prediction of the  $a_c(M_{\text{peak}})$  model is in reasonable agreement with the data. We note that this implies that all models that remove possible splashback halos will also be in agreement.

## 4 DISCUSSION

The main results of this paper are:

- The predictions of the age-matching model depend on how age is defined. More specifically, once tidal and splashback effects are removed from consideration by use of  $M_{\text{peak}}(z)$  rather than  $M_h(z)$ , the amount of assembly bias is reduced. This has the largest effect on low-mass halos  $M_h \lesssim 10^{12} h^{-1} M_\odot$ .
- At low galaxy mass,  $M_* \lesssim 10^{10} M_\odot/h^2$ , the results are consistent with little-to-no assembly bias, implying no relationship between halo age and galaxy quenching for central galaxies.
- At higher galaxy masses, the results are consistent with predictions from the age-matching model after removing the effects of splashback halos by using  $M_{\text{peak}}(z)$  to characterize formation history.

The first point is important for properly framing our expectations from assembly bias and the age-matching model. The extreme assembly bias predictions at low masses are driven by tidal and splashback effects lowering the present-day mass of the halo relative to its peak value at some earlier time. Wetzel et al. (2014) shows that the galaxies within these halos are not immediately affected by these encounters: after accretion onto a larger halo, the galaxy evolves as though it were still in the field for 3-5 Gyr. Most halos will be reaccreted by the larger halo during that time, and all will eventually be reaccreted onto the larger halo. There is a measurable increase in the quenched fraction within a couple virial radii of a larger halo, but splashback galaxies are not a significant contributor to the whole population of central galaxies on the red sequence. Thus standard age-matching predictions generally overestimate the impact of halo formation history on galaxy quenching. One aspect of the age-matching model that has received little attention (and this work is no different) is the possibility of scatter in any halo age-galaxy age correlation. A one-to-one correspondence between these two properties is unlikely, and scatter is a key component of the standard abundance matching model. Scatter between halo age and galaxy age would reduce the amplitude the assembly bias in the galaxy pop-

ulation. It is possible that a physically reasonable amount of scatter could reconcile the standard age-matching model with observations at high  $M_*$ . More work is required to define ‘physically reasonable scatter’, but at low masses the amount of scatter required to bring age-matching into agreement with the data would be so large as to eliminate any effective correlation.

The measurements of  $f_Q^{\text{en}}(\rho)$  cannot be reconciled with the predictions of the age-matching model at low  $M_*$ . This result caps a number of other results that are mutually exclusive with a model that maps halo age onto galaxy age at these mass scales. Tinker et al. (2008) demonstrated that the sizes of voids in red and blue galaxies is consistent with galaxy color being independent of large-scale environment, and inconsistent with the level of assembly bias seen in red galaxies in, for example, the Croton et al. (2007) semi-analytic model. When comparing the results of age-matching models to measurements of galaxy clustering and galaxy-galaxy lensing, there are conflicting results in the literature. Hearin et al. (2014) show reasonable agreement between the age-matching model and measurements of color-dependent clustering and lensing. In contrast, Mandelbaum et al. (2016) and Zu & Mandelbaum (2016) find that the predictions of the standard age-matching model are inconsistent with galaxy-galaxy lensing measurements split by color in bins of galaxy stellar mass. One difference between these two analyses is that Hearin et. al. compare models to data in thresholds of stellar mass, while the other papers compare models and data in bins of stellar mass. Additionally, Zehavi et al. (2011) use a standard halo occupation formalism to fit the color-dependent clustering of SDSS galaxies in multiple, narrow bins of color at fixed galaxy luminosity. In the standard HOD approach, galaxies occupy halos based only on the halo mass. Thus, if color depended significantly on halo age at fixed mass, the standard HOD approach would not be able to fit the clustering data. Zentner et al. (2014), using mock galaxy samples that contain assembly bias, do obtain a good fit to mock clustering using the standard HOD approach, but the clustering was measured in threshold samples, not magnitude bins as done in Zehavi et al. (2011).

The third point above implies that there is some change in how quenching correlates with halo formation history between low stellar masses and high stellar masses. Either that change manifests from a change in the physical mechanism that quenches galaxies, or that the mechanism is the same but the correlation between that mechanism and halo formation history—i.e., the scatter discussed above—increases significantly as halo mass decreases. Dalal et al. (2008) show that the assembly bias in low and high mass halos, split around  $M_h \sim 10^{12} M_\odot$ , is caused by different physical mechanisms. As we have noted above, assembly bias in low mass halos is driven by tidal encounters and other interactions with the large-scale environment. Assembly bias in high-mass halos, on the other hand, is imprinted in the primordial density field; early- and late-forming halos can be identified by the nature of their initial perturbations. The process that quenches low-mass field galaxies must be nearly independent of environment and thus uncorrelated with halo formation history. This does not necessarily imply that all the properties of low-mass field galaxies are uncorrelated with the details of halo growth; star formation rates, galaxy sizes, and

morphologies may correlate with short term or long term halo growth rates. The results here only indicate that the decision to migrate from the star-forming sequence to the red sequence is not up to the halo, after accounting for halo mass.

In contrast, high-mass galaxies tell a different story. Tinker (2016) shows that, if quenching is induced by a threshold in either galaxy mass or halo mass, the epoch of quenching will depend on halo formation history, with early-forming halos quenching earlier. Tinker et al. (2012) found that the clustering of x-ray groups depended on the state of the central galaxy; groups with star-forming centrals had higher clustering at  $z \sim 1$ . Halo assembly bias has also been, for the first time, robustly detected in observations of cluster sized halos (Miyatake et al. (2016); More et al. (2016)). The picture these results paint is consistent with the results here; older massive halos are more likely to contain quenched galaxies than younger halos, but the overall size of the effect is relatively small compared to the mean quenched fraction of high-mass galaxies.

We will tackle galactic conformity in a future paper in this series, but the results presented here are inconsistent with a model in which assembly bias creates strong large-scale galactic conformity for low-mass galaxies (i.e., conformity outside the virial radii of the halos in which the galaxies lie). There are, however, different definitions of galactic conformity that can lead to different quantitative results. In this paper, we focus on the quenched fraction of central galaxies, the same as the conformity definition used by Hearin et al. (2015). Kauffmann et al. (2013) measure conformity by measuring median star formation rates around samples of large isolated galaxies, where the isolated galaxies are divided into many bins based on their specific SFR. Kauffmann et al. (2013) find a strong suppression of sSFR of galaxies around the least star-forming isolated galaxies. The stellar mass range at which Kauffmann et al. (2013) find conformity is consistent with the stellar masses at which we find a weak trend of  $f_Q$  with  $\rho$ . It’s possible to change the mean sSFR without altering  $f_Q$ , thus further study is required to see if these observations are compatible. Additionally, a separate effect known as small-scale galactic conformity—the properties of satellite galaxies conforming to that of the central galaxy, first detected by Weinmann et al. (2006)—has been confirmed by other studies (Knobel et al. 2015; Kawinwanichakijet al. 2016; Berti et al. 2016).

A robust theory of galaxy formation must be consistent with all of these results listed above: a formation path that yields clear conformity within a dark matter halo, conformity of star formation rates outside of the halo, but limited to no correlation of the quiescent fraction on large-scale environment. A convincing explanation for all these observations will likely combine the influence of dark matter structure formation with complicated astrophysics and phenomena that is independent of halo formation. This series of papers will probe the limits of the influence of dark matter on present-day galaxy properties, separating—and hopefully simplifying—the problem of galaxy formation into those two regions.

The authors wish to thank Andrew Hearin for useful discussions. JLT acknowledges support from NSF grant AST-121189. ARW was supported by a Moore Prize Fellowship through the Moore Center for Theoretical Cosmology and Physics at Caltech and by a Carnegie Fellowship in Theoretical Astrophysics at Carnegie Observatories. CC acknowledges support from NASA grant NNX15AK14G, NSF grant AST-1313280, and the Packard Foundation.

## APPENDIX A: SUPPLEMENTARY HALO AGE DEFINITIONS

In this appendix we show results from two more common halo age proxies: the redshift at which half the halo mass forms,  $z_{1/2}$ , and halo concentration,  $c_{\text{vir}}$ .  $z_{1/2}$  is one of the most commonly used halo age definitions in the field, while  $c_{\text{vir}}$  is also widely used as a proxy for halo age, given that halo clustering correlates well with  $c_{\text{vir}}$  at fixed  $M_h$ , and that  $c_{\text{vir}}$  can be measured for halos in a single snapshot, without having to create full halo growth histories.

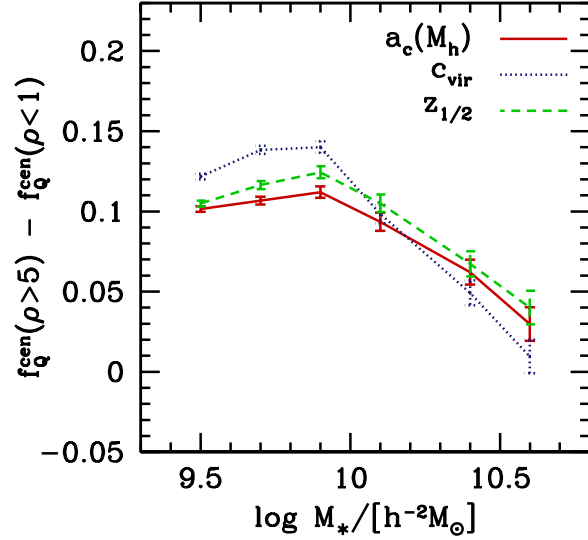
Figure A1 reprises the assembly bias results shown in Figure 7, only now including the two new halo age proxies listed above. The figure also shows the change in  $f_Q^{\text{cen}}$  for the  $a_c(M_h)$  age-matching model, for reference. There are slight quantitative differences in the assembly bias induced using these two halo age proxies, but the overall results are in good agreement with the fiducial age definitions used in the main text.

Figure A2 shows the ‘break point’ between halos being classified as ‘old’ and ‘young’ for each of our halo age proxies. The use of quotes around these terms is meant to stress that there is possibly no physical significance to these values—they are somewhat arbitrary dividing lines in continuous distributions of halo properties. But it is of interest to document the values required to match the observed values of  $f_Q^{\text{cen}}$  as a function of  $M_*$ . The top panel shows the break point when using fractional growth as our age proxy; i.e., halos of  $M_h \sim 10^{11.4} h^{-1} M_\odot$  (which house galaxies of  $m_{\text{gal}} \sim 10^{9.5} M_\odot/h^2$ ), contain quenched galaxies if their fractional growth rate is less than 17%, when measured from  $z = 0.8 \rightarrow 0$ . The middle panel shows the results using our halo formation epoch estimates:  $a_c(M_h)$ ,  $a_c(M_{\text{peak}})$ , and  $z_{1/2}$ . We note that the formation epoch for halos using  $z_{1/2}$  is much smaller than when using  $a_c$ , but the amplitude and nature of the assembly bias is nearly the same. In the bottom panel, we show the values of  $c_{\text{vir}}$  that delineate old from young halos.

We note that the values shown for the  $a_c$  model in Figure A2 are significantly smaller than those in the published version of Hearin & Watson (2013) (their Figure 2). An updated version of their Figure 2, which will be submitted as an erratum, are in good agreement with our results (A. Hearin, private communication). We also note that the absolute values of the break points do not alter the rank-ordering of the halos, and the results of their paper are unchanged.

## REFERENCES

Abazajian K. N., et al., 2009, *ApJS*, 182, 543  
 Abbas U., Sheth R. K., 2006, *MNRAS*, 372, 1749



**Figure A1.** Same as Figure 7, but now showing the results for halo age-matching models in which halos are rank-ordered by  $z_{1/2}$  and  $c_{\text{vir}}$ . For comparison, the model that uses  $a_c(M_h)$  is also shown.

Baldry I. K., Balogh M. L., Bower R. G., Glazebrook K., Nichol R. C., Bamford S. P., Budavari T., 2006, *MNRAS*, 373, 469  
 Bamford S. P., Nichol R. C., Baldry I. K., Land K., Lintott C. J., Schawinski K., Slosar A., Szalay A. S., Thomas D., Torki M., Andreescu D., Edmondson E. M., Miller C. J., Murray P., Raddick M. J., Vandenberg J., 2009, *MNRAS*, 393, 1324  
 Behroozi P. S., Wechsler R. H., Conroy C., 2013, *ApJ*, 770, 57  
 Behroozi P. S., Wechsler R. H., Wu H.-Y., 2013, *ApJ*, 762, 109  
 Behroozi P. S., Wechsler R. H., Wu H.-Y., Busha M. T., Klypin A. A., Primack J. R., 2013, *ApJ*, 763, 18  
 Berti A. M., Coil A. L., Behroozi P. S., Eisenstein D. J., Bray A. D., Cool R. J., Moustakas J., 2016, *ApJ*, submitted, ArXiv:1608.05084  
 Blanton M. R., Eisenstein D., Hogg D. W., Schlegel D. J., Brinkmann J., 2005, *ApJ*, 629, 143  
 Blanton M. R., Moustakas J., 2009, *ARA&A*, 47, 159  
 Blanton M. R., Roweis S., 2007, *AJ*, 133, 734  
 Blanton M. R., Schlegel D. J., Strauss M. A., Brinkmann J., Finkbeiner D., Fukugita M., Gunn J. E., Hogg D. W., Ivezić Ž., Knapp G. R., Lupton R. H., Munn J. A., Schneider D. P., Tegmark M., Zehavi I., 2005, *AJ*, 129, 2562  
 Brinchmann J., Charlot S., White S. D. M., Tremonti C., Kauffmann G., Heckman T., Brinkmann J., 2004, *MNRAS*, 351, 1151  
 Campbell D., van den Bosch F. C., Hearin A., Padmanabhan N., Berlind A., Mo H. J., Tinker J., Yang X., 2015, *MNRAS*, 452, 444  
 Chabrier G., 2003, *PASP*, 115, 763  
 Conroy C., Wechsler R. H., 2009, *ApJ*, 696, 620

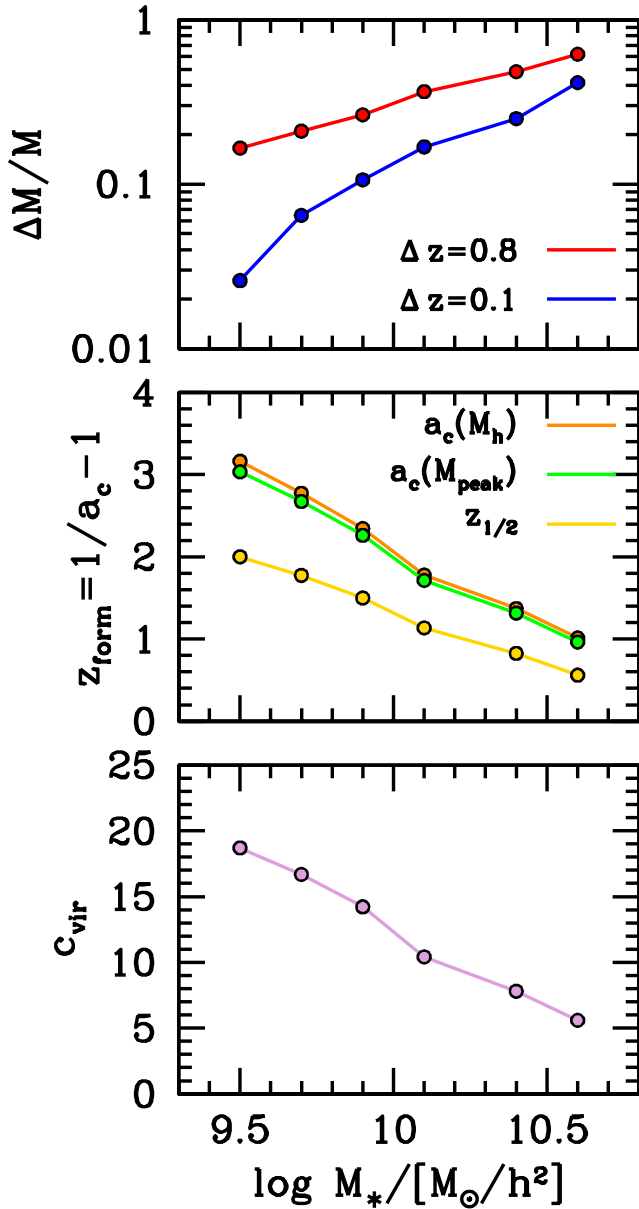


**Figure A2.** Each panel shows the break point between halos categorized as ‘old’ and ‘young’ for each halo age proxy. For each galaxy stellar mass, the old fraction is set to match the observed quenched fraction for central galaxies. *Top Panel:* Break point dividing old and young halos as determined by their fractional growth. Results are shown for redshift baselines  $\Delta z = 0.8$  and  $\Delta z = 0.1$ . The trend of rising growth rate with  $\log M_*$  is due in small part to changing growth rates with halo mass, but mostly due to the rising  $f_Q^{\text{cen}}$  with  $\log M_*$ . *Middle Panel:* Break point using three different definitions of formation epoch as described in the text. *Bottom Panel:* Break point between old and young halos using  $c_{\text{vir}}$  as the age proxy.

Conroy C., Wechsler R. H., Kravtsov A. V., 2006, *ApJ*, 647, 201

Croton D. J., Gao L., White S. D. M., 2007, *MNRAS*, 374, 1303

Dalal N., White M., Bond J. R., Shirokov A., 2008, *ApJ*, 687, 12

Davis M., Geller M. J., 1976, *ApJ*, 208, 13

Dressler A., 1980, *ApJ*, 236, 351

Gao L., Springel V., White S. D. M., 2005, *MNRAS*, 363, L66

Gao L., White S. D. M., 2007, *MNRAS*, 377, L5

Geha M., Blanton M. R., Yan R., Tinker J. L., 2012, *ApJ*, 757, 85

Hearin A. P., Watson D. F., 2013, *MNRAS*, 435, 1313

Hearin A. P., Watson D. F., Becker M. R., Reyes R., Berlind A. A., Zentner A. R., 2014, *MNRAS*, 444, 729

Hearin A. P., Watson D. F., van den Bosch F. C., 2015, *MNRAS*, 452, 1958

Hogg D. W., Blanton M. R., Brinchmann J., Eisenstein D. J., Schlegel D. J., Gunn J. E., McKay T. A., Rix H., Bahcall N. A., Brinkmann J., Meiksin A., 2004, *ApJ*, 601, L29

Kauffmann G., Li C., Zhang W., Weinmann S., 2013, *MNRAS*, 430, 1447

Kauffmann G., White S. D. M., Heckman T. M., Ménard B., Brinchmann J., Charlot S., Tremonti C., Brinkmann J., 2004, *MNRAS*, 353, 713

Kawinwanichakij L., Quadri R. F., Papovich C., Kacprzak G. G., Labbé I., Spitler L. R., Straatman C. M. S., Tran K.-V. H., Allen R., Behroozi P., Cowley M., Dekel A., Glazebrook K., Hartley W. G., Kelson D. D., Koo D. C., Lee S.-K., Lu Y., Nanayakkara T., Persson S. E., Primack J., Tilvi V., Tomczak A. R., van Dokkum P., 2016, *ApJ*, 817, 9

Knobel C., Lilly S. J., Woo J., Kovač K., 2015, *ApJ*, 800, 24

Kravtsov A. V., Berlind A. A., Wechsler R. H., Klypin A. A., Gottlöber S., Allgood B., Primack J. R., 2004, *ApJ*, 609, 35

Lacerna I., Padilla N., Stasyszyn F., 2014, *MNRAS*, 443, 3107

Tinker J. L., Leauthaud A., Bundy K., George M. R., Behroozi P., Massey R., Rhodes J., Wechsler R. H., 2013, *ApJ*, 778, 93

Li Y., Mo H. J., Gao L., 2008, *MNRAS*, 389, 1419

Maller A. H., Berlind A. A., Blanton M. R., Hogg D. W., 2009, *ApJ*, 691, 394

Mandelbaum R., Wang W., Zu Y., White S., Henriques B., More S., 2016, *MNRAS*, 457, 3200

Masters K. L., Nichol R., Bamford S., Mosleh M., Lintott C. J., Andreescu D., Edmondson E. M., Keel W. C., Murray P., Raddick M. J., Schawinski K., Slosar A., Szalay A. S., Thomas D., Vandenberg J., 2010, *MNRAS*, 404, 792

Miyatake H., More S., Takada M., Spergel D. N., Mandelbaum R., Rykoff E. S., Rozo E., 2016, *Physical Review Letters*, 116, 041301

More S., Miyatake H., Takada M., Diemer B., Kravtsov A. V., Dalal N. K., More A., Murata R., Mandelbaum R., Rozo E., Rykoff E. S., Oguri M., Spergel D. N., 2016, *ArXiv e-prints*

Moster B. P., Naab T., White S. D. M., 2013, *MNRAS*,

- 428, 3121
- Moster B. P., Somerville R. S., Maubetsch C., van den Bosch F. C., Macciò A. V., Naab T., Oser L., 2010, *ApJ*, 710, 903
- Oemler Jr. A., 1974, *ApJ*, 194, 1
- Park C., Choi Y.-Y., Vogeley M. S., Gott J. R. I., Blanton M. R., 2007, *ApJ*, 658, 898
- Reddick R. M., Wechsler R. H., Tinker J. L., Behroozi P. S., 2013, *ApJ*, 771, 30
- Skibba R., Sheth R. K., Connolly A. J., Scranton R., 2006, *MNRAS*, 369, 68
- Springel V., 2005, *MNRAS*, 364, 1105
- Swanson M. E. C., Tegmark M., Blanton M., Zehavi I., 2008, *MNRAS*, 385, 1635
- Swanson M. E. C., Tegmark M., Hamilton A. J. S., Hill J. C., 2008, *MNRAS*, 387, 1391
- Tinker J., Wetzel A., Conroy C., 2011, *MNRAS*, submitted, ArXiv:1107.5046
- Tinker J. L., 2016, *MNRAS*, submitted, ArXiv:1607.06099
- Tinker J. L., Conroy C., Norberg P., Patiri S. G., Weinberg D. H., Warren M. S., 2008, *ApJ*, 686, 53
- Tinker J. L., George M. R., Leauthaud A., Bundy K., Finoguenov A., Massey R., Rhodes J., Wechsler R. H., 2012, *ApJ*, 755, L5
- Tinker J. L., Leauthaud A., Bundy K., George M. R., Behroozi P., Massey R., Rhodes J., Wechsler R. H., 2013, *ApJ*, 778, 93
- Wang L., Weinmann S. M., De Lucia G., Yang X., 2013, *MNRAS*, 433, 515
- Wang Y., Yang X., Mo H. J., van den Bosch F. C., Weinmann S. M., Chu Y., 2008, *ApJ*, 687, 919
- Wechsler R. H., Bullock J. S., Primack J. R., Kravtsov A. V., Dekel A., 2002, *ApJ*, 568, 52
- Wechsler R. H., Zentner A. R., Bullock J. S., Kravtsov A. V., Allgood B., 2006, *ApJ*, 652, 71
- Weinmann S. M., van den Bosch F. C., Yang X., Mo H. J., 2006, *MNRAS*, 366, 2
- Wetzel A. R., Cohn J. D., White M., Holz D. E., Warren M. S., 2007, *ApJ*, 656, 139
- Wetzel A. R., Tinker J. L., Conroy C., Bosch F. C. v. d., 2014, *MNRAS*, 439, 2687
- Wetzel A. R., Tinker J. L., Conroy C., van den Bosch F. C., 2013, *MNRAS*, 432, 336
- Yang X., Mo H. J., van den Bosch F. C., 2006, *ApJ*, 638, L55
- Yang X., Mo H. J., van den Bosch F. C., Jing Y. P., 2005, *MNRAS*, 356, 1293
- York D. G., et al., 2000, *AJ*, 120, 1579
- Zehavi I., Zheng Z., Weinberg D. H., Blanton M. R., Bahcall N. A., Berlind A. A., Brinkmann J., Frieman J. A., Gunn J. E., Lupton R. H., Nichol R. C., Percival W. J., Schneider D. P., Skibba R. A., Strauss M. A., Tegmark M., York D. G., 2011, *ApJ*, 736, 59
- Zentner A. R., Hearin A. P., van den Bosch F. C., 2014, *MNRAS*, 443, 3044
- Zu Y., Mandelbaum R., 2016, *MNRAS*, 457, 4360